Engineering Journal issn: 0125-8281

Article

The Downstream of a Density-Stratified Sphere Wake

Karu Chongsiripinyo

Department of Mechanical Engineering, Faculty of Engineering, Chulalongkorn University, Bangkok 10330, Thailand
E-mail: Karu.C@chula.ac.th

Abstract. The objective of the present work is to access moderately-stratified wake statistics into the far downstream. This is accomplished via a continuation of the solution from the stratified-wake, body-inclusive, large-eddy simulation of [1] by a temporal-model, direct numerical simulation. Simulation of stratified sphere wake at $Re = U_\infty D/\nu = 10^4$ and $Fr = U_\infty/ND = 3$ is performed; U_∞, D, and N are sphere velocity, sphere diameter, and buoyancy frequency. Four findings are as follows. 1) Toward the end of the mid wake, centerline mean streamwise velocity deficit continues to decay with the power-law exponent $t^{-0.4}$; with $t = x/U_\infty$ is proportional to the distance (x) from the sphere. The progression of horizontal wake span is at $t^{1/3}$ but the vertical wake extent remains stagnant. 2) The beginning of transition into the late wake is found to be where the mean wake is geometrically most anisotropic. The transitioning is a gradual process that lasts $50 \leq Nt \leq 250$. 3) In the late wake, vertical profile of the defect velocity exhibits self-similarity. This self-similar state is not of Gaussian-type but better fitted with individual plane-wake self-similarity solution. The centerline defect velocity rapidly decays at a rate $t^{-3/4}$. Horizontal extension growth rate is reduced to $t^{1/4}$, disagreeing with many previous studies. The exponential growth rate of wake height is found to be $t^{1/2}$, an indication of the dominating viscous diffusion process. 4) Throughout the wake lifetime, deviation of density from the background state exists in the vertical center plane but small in magnitude. The deviation causes an enchancement in wake-core stratification that manifests itself until the transition into the late wake.

Keywords: Wakes, stratification, environmental fluid dynamics, computational fluid dynamics.

ENGINEERING JOURNAL Volume 25 Issue 5
Received 6 June 2020
Accepted 12 April 2021
Published 31 May 2021
Online at https://engj.org/
DOI:10.4186/ej.2021.25.5.1

DOI:10.4186/ej.2021.25.5.1

1. Introduction

Environmental fluid dynamics plays a substantial role in our lives and has become a subject of extensive investigation. This is because of its relevance to immediate problems such as atmospheric pollution and oceanic contamination, e.g., the ability to effectively predict and help redistribute air pollutants in a regional urban area requires a good understanding of the behavior of fluid motions in the atmosphere. Environmental flows are distinctive in their behaviors, that is the effects of gravity on a fluid of non-uniform density are inherently embedded. The non-uniform density distribution attribute, whose variation is generally in the vertical direction, is referred to as 'density stratification'. A planetary atmosphere or an ocean pycnocline, where the vertical gradient of mean density is negative, is known as stably-stratified environment. Stable stratification is known to suppress vertical motion, promote the formation of horizontal coherent eddies, and enable propagation of internal gravity waves.

Examination of the effects of density stratification on fluid motions is preferentially performed on canonical flows such as jets, wakes, or shear layers whose native behaviors are relatively well understood. The present article documents an examination of the late wake behind a sphere that has been subject to stable density stratification.

Stratified wakes behind an axisymmetric body evolve through, at least, three stages throughout their life spans. The multistage evolution was described in [2] and later categorized by [3].

During the first stage, stratified wakes grow as if in an unstratified fluid providing that the initial Froude number is $Fr = U_\infty/NL > O(1)$; here U_∞ is the body velocity relative to the background stream; L is the wake generator length scale; and N, known as the 'buoyancy frequency', is proportional to gravity and the vertical gradient of fluid density ($N^2 \propto -g(d\rho/dz)$). This is known as the three-dimensional (3D) regime or the 'near wake'.

Next, there is a transition period that exhibits an incident known as 'wake collapse' ([4] and [5]), where the vertical wake extent is suddenly reduced. The incident is simply one of the manifestations of the buoyancy effects that commences once the vertical Froude number, $Fr_V = U_0/NL_V$, is of $O(1)$ ([6]); U_0 is the wake centerline mean streamwise defect velocity and L_V is the vertical wake half-height. Stratified wakes then enter into the so-called non-equilibrium (NEQ) regime or the 'mid wake'. The NEQ regime is the most complicated among the three regimes because of intricate nonlinear interactions between turbulent motions and internal gravity waves ([7] and [8]).

Following the NEQ regime, the other transitioning happens where the emission of internal gravity waves has subsided ([7]). The last stage where stratified wakes become dominated by viscous mechanism is called the quasi-two-dimensional (Q2D) regime, or the 'late wake', that is characterized by the presence of thin eddy dipole structures, found to appear at $Nt \approx 250$ ([9] and [10]); here the time (t) is related to the downstream distance (x) from the wake generator via the Galilean transformation: $t = x/U_\infty$. The location in which the two transitions occur are quantified experimentally by [3] to be at $Nt = 2$ for the 3D-NEQ transitioning and at $Nt = 50$ for the NEQ-Q2D transitioning. Recently, some progress has been made in refining the categorization through dissecting stratified wakes into multiple parts: [6] differentiate the evolution of turbulence in the wake core from that of the mean wake; [11] decompose the $Fr = O(1)$ stratified wakes using 'Dynamic mode decomposition' (DMD); [12] look into turbulence anisotropy in the core of stratified wakes; and [13] employ a technique called 'Spectral proper orthogonal decomposition' (SPOD).

Numerical simulation has been utilized to investigate turbulent wakes in stratified fluid. A large part of our understanding comes from simulations that employ the so-called 'temporal approximation'. These temporal-model simulations are conducted in a laboratory frame. The computational volume resembles the field of view (with depth) of a stationary camera taking images of the wake from a lateral while the wake generator is being pulled along a fluid tunnel. The temporal model invokes the Galilean transformation that relates time in the reference "wake generator frame" to distance from the wake generator in the laboratory frame. An important assumption the model makes is the periodicity in the domain streamwise direction and the rationale behind is that the domain's streamwise span is much smaller than the total length of the wake ([14]).

The temporal model has extensively been utilized with success (e.g., [7, 9, 14–19] among others). While this type of simulation is, in general, computationally much more affordable than a body-inclusive simulation (e.g., [20–23]), the disadvantage is that, since a wake generator is absent, one has to prescribe an initial condition. Initial conditions used are generally an axisymmetric Gaussian-type profile of streamwise velocity superimposed with small-scale fluctuations, which unrealistically represents stratified wakes with $Fr = O(1)$ whose geometries are immediately asymmetric in the lee of a body. In attempts to tackle this problem, [24] conducts a temporal-flow simulation with a relevant initial condition by symmetrically extending a sub-domain from a body-inclusive simulation and [25] work around the problem by continuing the solution of a body-inclusive

simulation with a spatially-evolving model.

In the present study, the moderately-stratified ($Fr = O(1)$) wake solution of [1] is carried onto the far downstream with a temporal-model simulation. Figure 1 illustrates the problem under consideration with a cylindrical computational domain being used for the stratified wake to continue evolving onward. The ability to carry on the solution allows a more confident interpretation of wake statistics. We offer a method in constructing an initial condition which, to the best of the author's knowledge, is novel. The article begins with a theoretical prediction of late wakes in stratified fluid in section 2. Section 3 discusses the numerical techniques used to simulate the stratified wake. Section 4 addresses mean statistics including mean streamwise velocity deficit, wake extents, and vertical density profiles. The results of the study are summarized in section 5.

2. Prediction

We begin with a theoretical prediction of the late wake in a stratified fluid. The following derivation presented in subsection 2.1, while relies on heavy assumptions, offers an alternative view into stratified wake behavior. Specifically, the analysis reveals that a late-wake vertical profile of the mean streamwise velocity deficit is not Gaussian but similar to that of a two-dimensional plane wake. Followed by the analysis, subsection 2.2 presents a usage of the plane-wake profile, as opposed to the Gaussian profile, in predicting the evolutions of centerline mean streamwise defect velocity and wake extents.

2.1. Non-Gaussian Velocity Profile

The incompressible Navier-Stokes equations under the Boussinesq approximation can be written as

$$\frac{\partial \boldsymbol{u}^*}{\partial t^*} + \boldsymbol{u}^* \cdot \boldsymbol{\nabla}^* \boldsymbol{u}^* = -\frac{1}{\rho_0^*}\boldsymbol{\nabla}^* p^* + \nu^* \boldsymbol{\nabla}^{*2}\boldsymbol{u}^* - \frac{\rho_d^*}{\rho_0^*} g^* \boldsymbol{e_z}. \quad (1)$$

The asterisk superscript denotes dimensional quantities. Coordinate axes x, y, and z denote streamwise, spanwise, and vertical directions (see Fig. 1). ν^* is kinematic viscosity. Density is decomposed as follows: $\rho^*(x_i, t) = \rho_0^* + \rho_{bg}^*(z) + \rho_d^*(x_i, t)$; here ρ_0^* is a constant reference density, $\rho_{bg}^*(z)$ is a linearly varying deviation of the background, and $\rho_d^*(x_i, t)$ is a flow-induced density deviation.

In the context of wake flow, averaging the streamwise component of Eq. (1) after the dependent variables are Reynolds-decomposed ($\phi = \langle\phi\rangle + \phi'$, where ϕ is an instantaneous realization) and assuming that turbulent diffusion is negligible in the far downstream (i.e., small with respect to viscous diffusion) yield

$$\boldsymbol{U}^* \cdot \boldsymbol{\nabla}^* \boldsymbol{U}_{\boldsymbol{x}}^* = \nu^* \boldsymbol{\nabla}^{*2} \boldsymbol{U}_{\boldsymbol{x}}^*; \quad (2)$$

where $\boldsymbol{U}^* = \langle \boldsymbol{u}^* \rangle$ is the mean velocity. The operator $\langle\phi\rangle$ averages ϕ in time which, for a statistically-stationary problem, is identical to an ensemble-average operator.

Equation (2) is nondimensionalized using sphere velocity (U_∞^*) as a characteristic streamwise velocity and centerline mean streamwise defect velocity ($U_0^* = U_d^*(y = z = 0)$) as a characteristic spanwise velocity. Reminding that velocity deficit $U_d^* = U_\infty^* - U_x^*$. By following [26–29], vertical velocity is scaled by $U_0^* Fr_H^2/\alpha$; with $Fr_H = U_0/NL_H$ is horizontal Froude number; $\alpha = L_V/L_H$ is mean wake geometrical aspect ratio; L_V and L_H are vertical and horizontal mean wake half-spans, that are also used as characteristic vertical and horizontal length scales, respectively.

The vertical wake extent or wake half-height (L_V) measures a vertical distance from the centreline to a position on the wake cross-section where U_d is reduced to half of its centreline value and the horizontal wake extent or wake half-width (L_H) is defined synonymously but in the horizontal direction. Time is scaled by L_H^*/U_∞^*. The scaled Equation (2) is then written as

$$U_x \frac{\partial U_x}{\partial x} + \left(\frac{U_0^*}{U_\infty^*}\right) U_y \frac{\partial U_x}{\partial y} + \left(\frac{U_0^*}{U_\infty^*} Fr_V\right) U_z \frac{\partial U_x}{\partial z} = \frac{1}{Re_H}\left(\frac{U_0^*}{U_\infty^*}\right)\left(\frac{\partial^2 U_x}{\partial x^2} + \frac{\partial^2 U_x}{\partial y^2} + \frac{1}{\alpha^2}\frac{\partial^2 U_x}{\partial z^2}\right); \quad (3)$$

with $Re_H = U_0 L_H/\nu$, the Reynolds number which decreases over the wake lifetime and $Fr_V = U_0/NL_V$, the vertical Froude number signifying the competition between buoyancy time scale and vertical advection time scale.

In the downstream, deficit velocity is small relative to the sphere velocity ($U_0^*/U_\infty^* \ll 1$) and $Fr_V = O(1)$ according to [6]. Also by the nature of stratified flow in which the vertical length scale is smaller than the horizontal length scale ($\alpha < 1$), the horizontal diffusion terms are negligible with respect to the vertical diffusion term. This leads us to the one-dimensional diffusion equation,

$$\frac{\partial U_x}{\partial t} = \frac{1}{\alpha^2 Re_H}\left(\frac{U_0^*}{U_\infty^*}\right)\frac{\partial^2 U_x}{\partial z^2}; \quad (4)$$

here, the temporal acceleration term ($\partial U_x/\partial t$) stems from the streamwise convection term ($U_x \partial U_x/\partial x$) in Eq. (3) for $t = x/U_\infty \simeq x/U_x$ is directly proportional to the distance from a wake generator to the temporal frame. t is now strictly of the temporal frame, as opposed to the variable t in Eq. (1) which describes time

in both frames. It is important to emphasize that temporal averaging in spatially-evolving, wake generator frame during a steady state (statistically-stationary process) is identical to the ensemble averaging in temporal, moving frame (transient process).

Substituting $U_x = U_\infty - U_d$, rewriting Eq. (4) in dimensional form and dropping the asterisk give

$$\frac{\partial U_d}{\partial t} = \nu \frac{\partial^2 U_d}{\partial z^2}. \quad (5)$$

At this point, we look for a self-similarity solution of the form $U_d = At^{-n} f(z/(\nu t)^{1/2})$ where A is a constant and f is a function to be found. To solve Eq. (5), two boundary conditions and one initial condition are required. While it is clear that $U_d(z \to \pm\infty, t) = 0$ are two boundary conditions, an initial condition is not as straightforward. If our wake generator is modeled to be infinitesimal but, yet, can deposit momentum deficit in the wake, a sensible initial condition takes the form $U_d(z, t = 0) = \delta_m(z)$ where δ_m is a modified Dirac delta function with its characteristic integration is proportional to the wake momentum deficit. This problem is, thus, posted similarly to the one-dimensional diffusion problem of infinitely thin vortex sheet: $\partial_t \omega_y = \nu \partial_{zz} \omega_y$ subjected to initial velocity field $U_x(z > 0, t = 0) = U$ and $U(z < 0, t = 0) = -U$ ([30]). By modeling our problem as such, we introduce $\Lambda(z, t) = \int_0^z U_d(z', t) dz'$ with its physical meaning being a sign cumulative deficit volume flow rate per unit spanwise depth. Let $\pm\Lambda_0 = \Lambda(z \to \pm\infty, t)$; where Λ_0 is a positive constant. Since the deficit volume flow rate is initially taken to be "concentrated" at $z = 0$, it follows that $\Lambda(z > 0, t = 0) = \Lambda_0$ and $\Lambda(z < 0, t = 0) = -\Lambda_0$. The self-similarity solution that helps explain how the velocity deficit decays by purely diffusive transport is therefore

$$\frac{U_d(z,t)}{U_0(t)} = e^{-z^2/4\nu t}; \quad U_0(t) = \frac{\Lambda_0}{\sqrt{\pi \nu t}}. \quad (6)$$

The vertical half-wake span can be found by setting $e^{-L_V^2/4\nu t} = 0.5$. This leads to $L_V = \sqrt{4ln2}(\nu t)^{1/2}$. Substituting $\nu t = L_V^2/4ln2$ into the νt argument of the exponential function in Eq. (6) gives

$$\frac{U_d(z,t)}{U_0(t)} = e^{-ln2(z^2/L_V^2)}. \quad (7)$$

Equation (7) indicates that, under our assumptions for the far downstream wake, the mean wake vertical self-similarity profile is not of Gaussian type. This solution reminds us of the self-similarity solution of a plane wake, $f(\xi) = e^{-\lambda \xi^2}$ where $f(\xi)$ is the self-similar profile with $\lambda = ln2$ ([31]).

Before we continue with the next subsection, the result deserves a brief discussion. Upon substituting $\sqrt{\nu t} = L_V \sqrt{4ln2}^{-1}$ into $U_0(t) = \Lambda_0/\sqrt{\pi \nu t}$, the resulting $U_0(t) L_V(t) = \sqrt{4ln2/\pi}\Lambda_0$ would violate the conservation of momentum in which it is $U_0 L_V L_H$ and not $U_0 L_V$ that is constant ([32]). This is expected because of our substantial simplification that omits all horizontal processes. One could modify the analysis by "relaxing" Λ_0 so as not to be held constant (e.g., to be inversely proportional to L_H providing that L_H is a weak function of time with respect to $t^{1/2}$) in order to account for the change in the vertical-integral flux deficit caused by the change in the flux deficit in the horizontal due to the continuous growth of L_H. However in doing so, one would sacrifice the presumption of the strictly self-similarity solution.

2.2. Plane-wake Estimate

An analytical prediction of wake height, wake width, and defect velocity is provided by [32] using a simplified momentum equation based on the Gaussian similarity profile. In this section, we follow [32] but rather with a velocity profile that is suggested by the previous subsection. Profile of mean streamwise defect velocity is presumed to take the form:

$$U_x = U_\infty - U_0 e^{-C(y^2/2L_H^2 + z^2/2L_V^2)}; \quad (8)$$

with $C = 2\ln 2$ for the plane-wake profile (PW) and $C = 1$ for the Gaussian profile (GP).

Following [32], a simplified form of mean streamwise momentum equation in the far field is

$$U_\infty \frac{\partial U_x}{\partial x} = \nu_{ey} \frac{\partial^2 U_x}{\partial y^2} + \nu_{ez} \frac{\partial^2 U_x}{\partial z^2}. \quad (9)$$

Notice that Eq. (9) can be obtained in the similar fashion as Eq. (4) but without omitting the spanwise advection by turbulence and the spanwise molecular diffusion. In Eq. (9), $\nu_{ey} = \nu + \nu_t$ and $\nu_{ez} = \nu$ are effective kinematic viscosities. The turbulent viscosity (ν_t) is defined as in $\langle u_x' u_y' \rangle = \nu_t \partial U_x/\partial y$. [33] found that $U_0 L_H/\nu_t \approx 15$ beyond the buoyancy period of $Nt = 100$.

Substituting Eq. (8) into Eq. (9) gives an equation containing three types of terms whose valuations depend on different independent variable (y, z, or neither). Grouping terms for each of the type yields a set of three relations whose solutions reflect the constraint that Eq. (9) places on Eq. (8). The presumed plane-wake profile is a solution of the resulting relations if the following equations hold:

$$\frac{1}{CU_0}\frac{dU_0}{dx} = -\frac{\nu_{ey}}{L_H^2 U_\infty} - \frac{\nu_{ez}}{L_V^2 U_\infty},$$
$$\frac{1}{C}\frac{dL_H}{dx} = \frac{\nu_{ey}}{U_\infty L_H}, \quad \frac{1}{C}\frac{dL_V}{dx} = \frac{\nu_{ez}}{U_\infty L_V}. \quad (10)$$

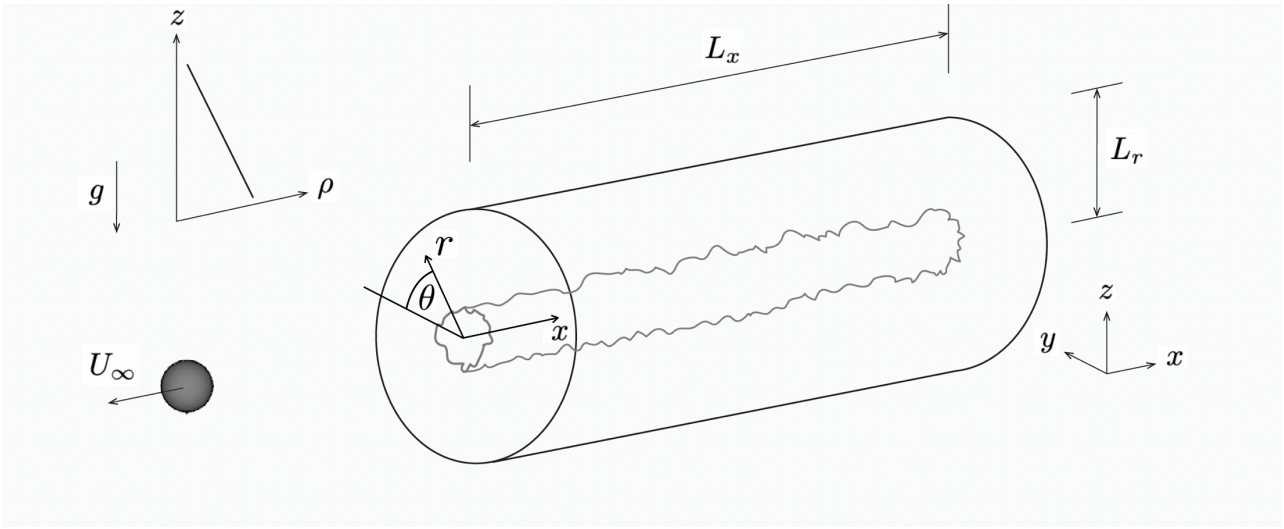

Fig. 1. Problem under consideration. The sphere is towed with velocity U_∞ away from a cylindrical, laboratory-frame "test section" of size $L_x \times L_r$ in dimensions. In the temporal model, this 'stationary' test section is replaced by a computational domain. Computation is conducted to evolve the sphere wake in the absence of the sphere itself.

Interested readers is referred to [33] for a detailed explanation on how to obtain Eq. (10). The set of equations, Eq. (10), is numerically marched for L_H and L_V then U_0 is calculated by enforcing the conservation of momentum, $U_0 = U_B D_m^2/8L_H L_V$ ([32]); here $D_m^2 = CD^2 c_D/2$ and $c_D = 0.29$, the drag coefficient from the body-inclusive simulation ([1]). It is worth mentioning that, thus, while L_H and L_V are numerically identical initially for the two profiles, U_0 are not. To allow a fair comparison with [32], the initial condition is chosen at $x = 6D$ although the domain of applicability resides in the downstream. The resulting theoretically-estimated (TE) velocity deficit and wake extents will be discussed along with results from the simulation.

3. Simulation

The incompressible Navier-Stokes equations under the Boussinesq approximation, Eq. (1), along with the continuity and the advection-diffusion equation for density, as follows:

$$\frac{\partial u_i^*}{\partial x_i^*} = 0; \quad \frac{\partial \rho^*}{\partial t^*} + u_j^* \frac{\partial \rho^*}{\partial x_j^*} = \kappa^* \frac{\partial^2 \rho^*}{\partial x_j^* \partial x_j^*}; \tag{11}$$

where κ^* is density diffusivity, are non-dimensionalized using the following dimensionless variables:

$$t = \frac{t^* U_\infty^*}{D^*}, \quad x_i = \frac{x_i^*}{D^*}, \quad u_i = \frac{u_i^*}{U_\infty^*},$$
$$\rho = \frac{\rho^*}{\rho_0^*}, \quad \rho_d = \frac{\rho_d^*}{-D^* d\rho_{bg}^*/dz^*}, \quad p = \frac{p^*}{\rho_0^* U_\infty^{*2}}. \tag{12}$$

Substituting Eq. (12) into Eq. (1) and Eq. (11), the non-dimensional set of equations is

$$\frac{\partial u_i}{\partial t} + u_j \frac{\partial u_i}{\partial x_j} = -\frac{\partial p}{\partial x_i} + \frac{1}{Re} \frac{\partial^2 u_i}{\partial x_j \partial x_j} - \frac{1}{Fr^2} \rho_d \delta_{i3};$$
$$\frac{\partial u_i}{\partial x_i} = 0; \quad \frac{\partial \rho}{\partial t} + u_j \frac{\partial \rho}{\partial x_j} = \frac{1}{RePr} \frac{\partial^2 \rho}{\partial x_j \partial x_j}. \tag{13}$$

The relevant non-dimensional parameters are as follows: the Reynolds number, $Re = U_\infty D/\nu = 10^4$, the Prandtl number, $Pr = \nu/\kappa = 1$, and the Froude number, $Fr = U_\infty/ND = 3$. The buoyancy frequency is defined by $N^* = [-g^*(d\rho_{bg}^*/dz^*)/\rho_0^*]^{1/2}$. The non-dimensional buoyancy frequency is equivalently $N \equiv Fr^{-1}$.

The governing non-dimensional equations (Eq. 13) are first rewritten as in Eq.(14)-(18) and numerically solved in a cylindrical coordinate system on staggered grids. A combination of explicit and implicit schemes is used. Implicit marching by the second-order Crank-Nicolson scheme is performed for the azimuthal viscous terms to alleviate the stiffness of the discretized system. The remaining terms are marched explicitly using the third-order Runge-Kutta scheme. Periodic boundary condition in both the azimuthal and the streamwise directions reduces the discretized Poisson equation into inversion of a tridiagonal matrix. The tridiagonal matrix system is solved using a direct solver, [34]. The interested reader is advised to consult [35] for the detail on how the cylindrical coordinate system is employed and how the combination of the methods described above is

DOI:10.4186/ej.2021.25.5.1

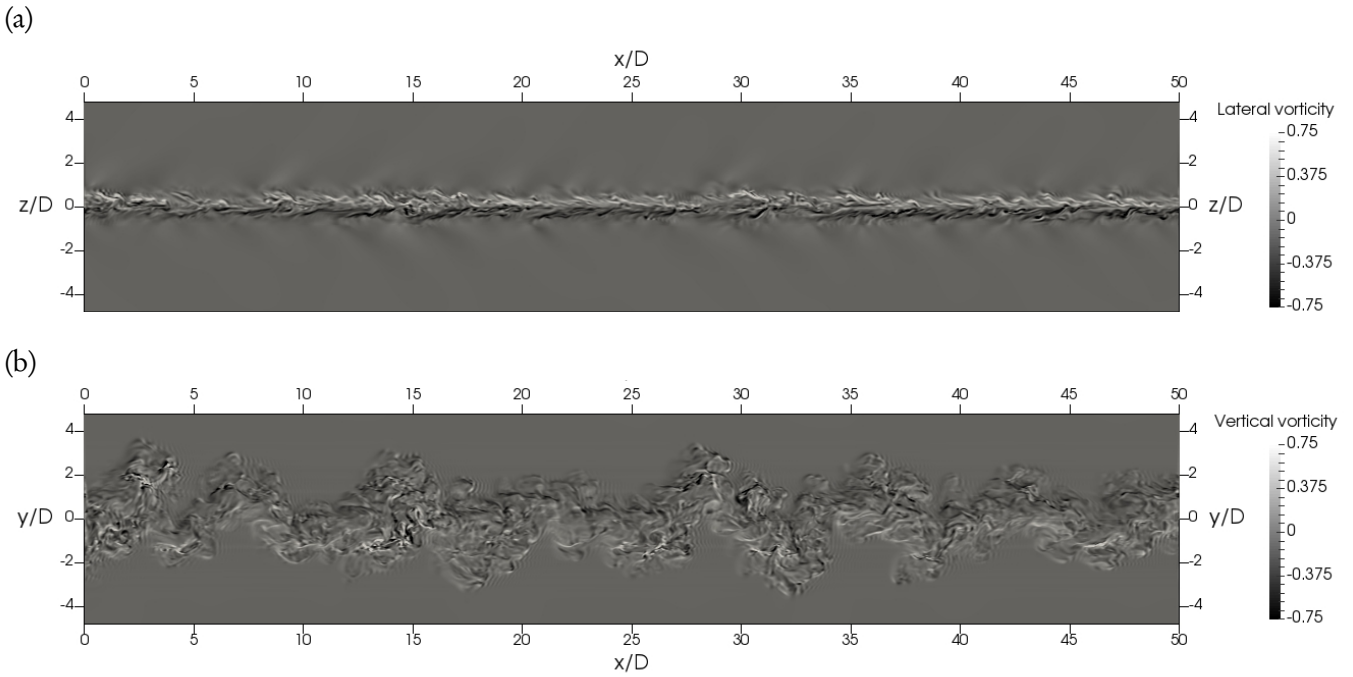

Fig. 2. Initial prescription of vorticity field. Lateral vorticity on the vertical centerline cut (a) and vertical vorticity on the horizontal centerline cut (b).

implemented.

$$\frac{1}{r}\frac{\partial r u_r}{\partial r} + \frac{1}{r}\frac{\partial u_\theta}{\partial \theta} + \frac{\partial u_x}{\partial x} = 0 \tag{14}$$

$$\frac{\partial \rho}{\partial t} + (\boldsymbol{u}\cdot\boldsymbol{\nabla})\rho = \frac{1}{RePr}\nabla^2\rho \tag{15}$$

$$\frac{\partial u_r}{\partial t} + (\boldsymbol{u}\cdot\boldsymbol{\nabla})u_r - \frac{u_\theta^2}{r} = -\frac{\partial p}{\partial r} + \frac{1}{Re}\left(\nabla^2 u_r - \frac{u_r}{r^2} - \frac{2}{r^2}\frac{\partial u_\theta}{\partial \theta}\right) - \frac{1}{Fr^2}\rho_d \sin\theta \tag{16}$$

$$\frac{\partial u_\theta}{\partial t} + (\boldsymbol{u}\cdot\boldsymbol{\nabla})u_\theta + \frac{u_r u_\theta}{r} = -\frac{1}{r}\frac{\partial p}{\partial \theta} + \frac{1}{Re}\left(\nabla^2 u_\theta - \frac{u_\theta}{r^2} + \frac{2}{r^2}\frac{\partial u_r}{\partial \theta}\right) - \frac{1}{Fr^2}\rho_d \cos\theta \tag{17}$$

$$\frac{\partial u_x}{\partial t} + (\boldsymbol{u}\cdot\boldsymbol{\nabla})u_x = -\frac{\partial p}{\partial x} + \frac{1}{Re}\nabla^2 u_x \tag{18}$$

where

$$\boldsymbol{u}\cdot\boldsymbol{\nabla} = u_r\frac{\partial}{\partial r} + \frac{u_\theta}{r}\frac{\partial}{\partial \theta} + u_x\frac{\partial}{\partial x}$$

$$\nabla^2 = \frac{1}{r}\frac{\partial}{\partial r}\left(r\frac{\partial}{\partial r}\right) + \frac{1}{r^2}\frac{\partial^2}{\partial \theta^2} + \frac{\partial^2}{\partial x^2}$$

Computational domain size is $L_x = 50.0$ in the streamwise direction, a 7 multiple of St^{-1} where $St = 0.14$ is the Strouhal number whose significance is related to large-scale vortex shedding from the sphere. In the radial direction, $L_r = 30.7$ to allow free propagation of internal gravity waves. The number of grid points are $N_x = 1280$, $N_r = 406$, and $N_\theta = 256$ that make up a total of 133 million grid points. The distribution of the computational grid is optimized on the basis of Kolmogorov length scale (η) where the initial field is constructed. The scale is calculated directly from the turbulent rate of dissipation (ε) by $\eta = (Re^3\varepsilon)^{-1/4}$; $\varepsilon = \nu\langle\partial_j u_i'\partial_j u_i'\rangle$. Since the Kolmogorov length scale increases towards downstream, the resolutions $\Delta r_{\text{centerline}}/\eta \approx 1$ and $\Delta x/\eta \approx 3$ for the initial condition suffice the choice in the absence of a turbulence model. The numerical resolution in time (time step) is dynamically calculated based on the Courant–Friedrichs–Lewy condition, chosen at CFL = 1, that results in $\Delta t \simeq 0.003$ at the beginning ($t = 28.27$) and $\Delta t \simeq 0.1$ at the end of the simulation ($t = 12900$).

The simulation is initialized using velocity and density fields from a single location at $x/D = 28.27$ from the body-inclusive simulation of [1]. An ensemble of 1200 cross-sectional snapshots of velocity and density are stacked in the streamwise direction of the present temporal-model computational volume. As far as we know, this is the first temporal-model simulation of stratified wake whose initial condition is prescribed using the stacking method. The location $x/D = 28.27$ is where the centerline mean defect velocity is 10% of the relative free-stream velocity similar to the peak deficit velocity that was used for the initialization of the

DOI:10.4186/ej.2021.25.5.1

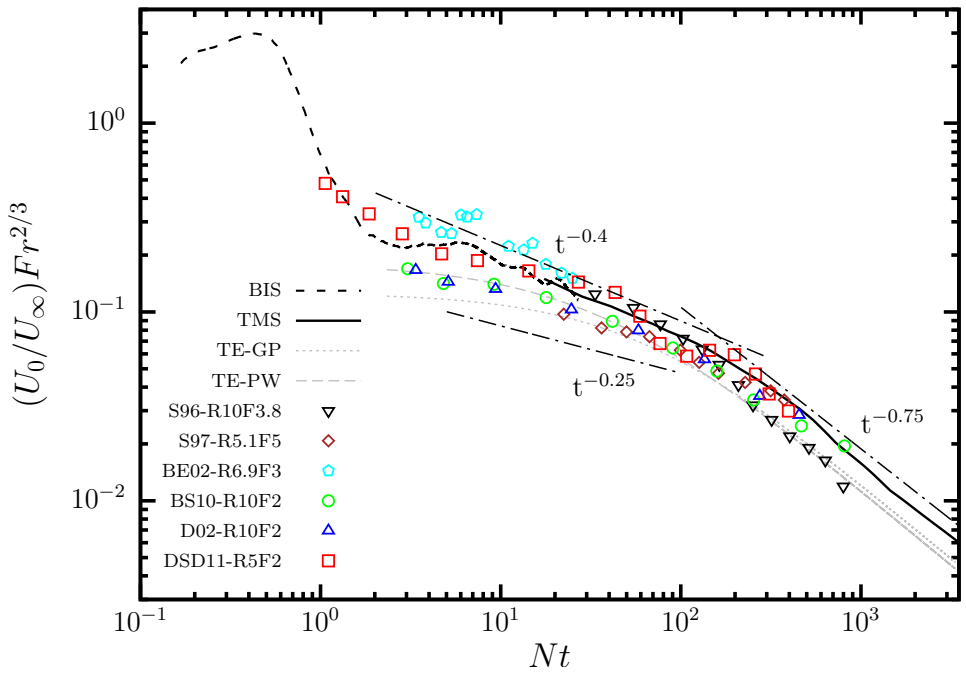

Fig. 3. History of the centerline mean streamwise velocity deficit. The dashed line (BIS) is from the body-inclusive simulation of [1]. The solid line (TMS) is the present work. Lines in grey are from the theoretical estimations derived in section 2; the dotted line (TE-GP) and dashed line (TE-PW) are predicted U_0 from the Gaussian profile and the plane-wake profile, respectively. Symbols are as follows: [S96-R10F3.8] refers to the data from the experiment of [36] at $(Re, Fr) = (10^4, 3.8)$; [S97-R5.1F5] refers to the data from the experiment of [3] at $(Re, Fr) = (5100, 5)$; [BE02-R6.9F3] refers to the data from the experiment of [37] at $(Re, Fr) = (6900, 3)$; [BS10-R10F2] refers to the data from the towed-wake simulation of [9] at $(Re, Fr) = (10^4, 2)$; [D02-R10F2] refers to the data from the simulation of [38] at $(Re, Fr) = (10^4, 2)$; [DSD11-R5F2] refers to the simulation of [39] at $(Re, Fr) = (5000, 2)$.

temporal-model simulation in [9] and small-scale eddies have sufficiently been dissipated such that the solution can be carried on without an artificial turbulence model. The other criterion is the presence of steady lee waves behind the sphere that induces the so-called 'oscillatory-modulation' ([1]). The location $x/D = 28.27$ is situated close the valley of the lee waves and thus vertical mean velocity is near zero. We note that this 'near zero' causes a slight discrepancy in the overlapped region between the upstream simulation and the present simulation. It is important to note that the mapping from a single location results in an absence of the steady lee waves. However if the mapping was done from data that span over a streamwise space of a body-inclusive simulation domain, it would violate the invoked Galilean transformation.

Figure 2 visualizes the initial condition in the form of vorticity field. Lateral vorticity is shown on the vertical centerline cut (a) and vertical vorticity shown on the horizontal centerline cut (b). The figure asserts the importance of constructing a moderately-stratified wake initial condition with non-axisymmetrical wake radial extent that is vertically thin but horizontally wide, in contrast to an axisymmetric velocity profile that have often been done.

The computation takes place in a small Linux workstation with 16 processors on 2x Intel® Xeon® E5-2670 and 128 Gigabytes of memory. From the 24/7 run, the simulation itself (post-processing excluded) consumes close to 2500 wall-clock hours or about 105 days in total.

4. Results

4.1. Velocity Deficit

Mean streamwise defect velocity along the centerline (U_0) of the present temporal-model simulation (TMS), shown in Fig. 3, continues to decay with a similar power law to that of the upstream body-inclusive simulation (BIS). The power-law decay in the NEQ regime is found to be close to $U_0 \propto t^{-0.4}$, in agreement with the previously reported value $t^{-0.38}$ from the experimental data of [41]. However, it is steeper than the reported values of $\approx t^{-0.25}$ from many previous works (e.g., [3], [9], [39], and [22]). The decay rate remains close to $t^{-0.4}$ until $Nt \approx 100$. Figure 3 shows that the NEQ-Q2D transitioning takes place gradually that progressively promotes the rate of U_0 decay from $t^{-0.4}$ to

DOI:10.4186/ej.2021.25.5.1

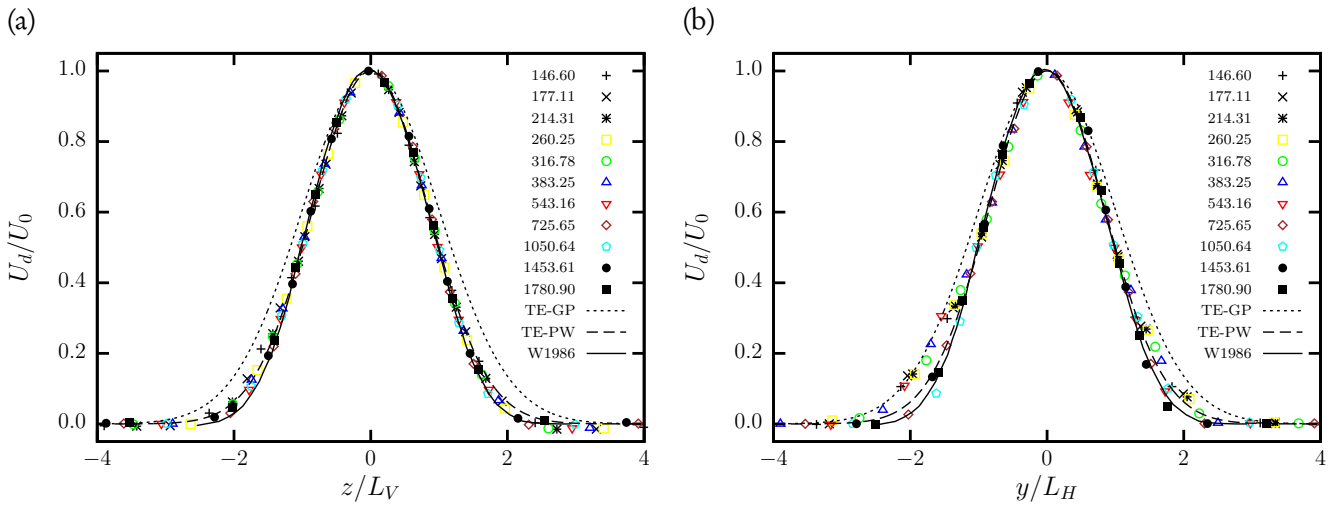

Fig. 4. Profiles of normalized mean streamwise velocity deficit in the vertical direction (a) and in the horizontal direction (b). A numeric legend is buoyancy period (Nt) at which the profile is extracted. W1986 refers to the two-dimensional wake experimental data of [40].

$t^{-0.75}$. The transitioning lasts until $Nt \approx 250$, which happens to be where [9] (and later [10]) found the appearance of emerging quasi-2D, pancake vortices. The power-law decay $t^{-0.75}$, consistent with the experimental data of [3] during the Q2D regime, remains intact until the termination of our simulation at $Nt \approx 3500$.

In the downstream where the theoretical estimation is applicable, both of the predictions capture the downstream power law ($t^{-0.75}$) reasonably well and the magnitude difference between the predicted U_0s from both of the profiles is small.

Lateral distributions of normalized mean streamwise velocity deficit at various downstream locations are shown in Fig. 4 (a) for vertical profiles and Fig. 4 (b) for horizontal profiles. It is obvious that the vertical profiles are self-similar and of the plane-wake distribution rather than of Gaussian distribution. Interestingly, the horizontal profiles appear to also be of the plane-wake distribution, especially at far downstream. This evidence strengthen the validity of our presumption (Eq. 8) with $C = 2ln2$.

4.2. Wake Dimensions

From here we turn our attention into vertical and horizontal wake extents, shown in Fig. 5. Before diving into the result from the present simulation, it is noticeable that at the immediate lee of the sphere ($Nt \approx 0.167$), the fact that L_V is already smaller than L_H indicates an absence of the three-dimensional regime. In fact, $L_V \neq L_H$ remains true until the termination of our simulation. Thus, one should take into account the mean wake geometrical asymmetry into the initial condition not only for which $Fr < O(1)$ but also at $Fr = O(1)$. During the NEQ regime after the present simulation is initiated, $10 \leq Nt \leq 50$, the wake half-height remains 'locked' at $L_V/D \approx 0.31$ and the wake half-width continues to increase with an exponential growth rate of approximately $L_H \propto t^{1/3}$. The vertical extent then starts increasing at about $Nt \approx 50$ which is where the NEQ-Q2D transitioning takes place according to [3]. The increase in L_V from its bottom position (locked value) that is accommodated by a decrease in L_H thus forms a valley of the wake geometrical aspect ratio, $\alpha = L_V/L_H$, at $Nt \simeq 50$, shown in Fig. 6.

The geometry of the mean wake is also most anisotropic at $Nt \simeq 50$ where the aspect ratio is found to be $L_V/L_H \simeq 0.15$. This local minimum of α can, therefore, be used as an indicator of where the NEQ-Q2D transitioning commences. It is worth mentioning that it is the wake half-lengths, especially the asymptote towards the viscous length scale of L_V ($L_V \propto t^{1/2}$), that first signals the NEQ-Q2D transitioning rather than the promotion of the U_0 rate of decay. Figure 5 shows that L_V of [9] and [38] also start to increase at around $Nt \approx 50$ but the drop in L_H is not obvious in their results.

In the downstream (Q2D) region, the overall growth of horizontal wake-width is found to be close to $L_H \propto t^{1/4}$, that makes $U_0 L_V L_H$ satisfies the conservation of momentum with its power-law exponent, in that $U_0 L_V L_H \propto t^{-3/4} t^{1/2} t^{1/4} \propto t^0$. This lateral growth rate, while in agreement with [32] whose theoretical analysis reveals $L_H \propto t^{1/4}$ during the Q2D regime, disagrees with many previous numerical simulations that were conducted using the similar, temporal approximation. This includes numerical simulations of [9], [38],

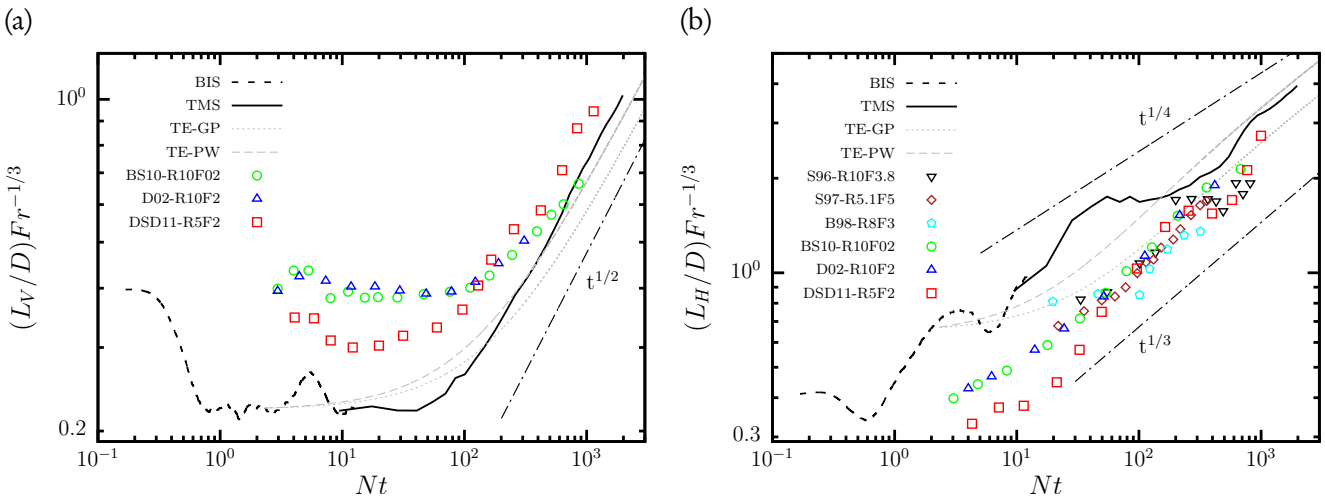

Fig. 5. The evolution of wake height (L_V) and of wake width (L_H). Symbols as in Fig. 3 with an additional symbol as follows: [B98] refers to data from the experiments of [42] at $(Re, Fr) = (8000, 3)$.

and [39] whose L_H growth rates are rather at $t^{1/3}$. Further investigation is required to answer the following question: Of what characteristics in the temporal-model initial condition that stems from the presence of the body that drives the growth rate to be $L_H \propto t^{1/4}$ rather than $L_H \propto t^{1/3}$?

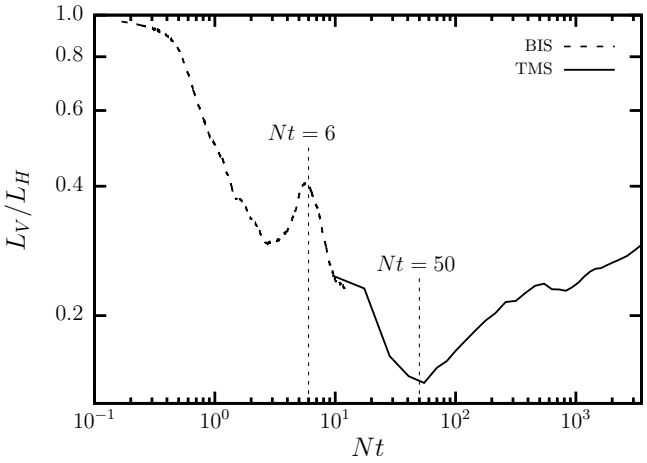

Fig. 6. Geometrical mean wake aspect ratio of vertical wake span to horizontal wake span (L_V/L_H).

Our theoretical prediction shows that L_V from the plane-wake, U_d profile (TE-PW) asymptotes toward $\sqrt{4ln2}(\nu t)^{1/2}$ while that of the Gaussian, U_d profile (TE-GP) asymptotes toward $\sqrt{2}(\nu t)^{1/2}$. For both of the profiles, it is expected that the L_V growth rate has to finally be $t^{1/2}$ since, from our derivation, the far wake vertically expands by diffusion solely via viscosity. It is found that L_V of the theoretically-estimated TE-PW is indeed closer to L_V from the present simulation in comparison to that from the Gaussian profile. The magnitude "Error" of the predicted L_V comes from the absence of vertical convection either from mean convection or turbulence convection (i.e., Reynolds stress: $\partial\langle u'w'\rangle/\partial z$). In terms of horizontal wake half-width, while both of L_H from the theoretically-estimated TE-PW and TE-GP are close to L_H from the present simulation, their growth rate is rather $t^{1/3}$ and not $t^{1/4}$. Further investigation is required to determine the robustness of $L_H \propto t^{1/4}$ at farther downstream. This can be done via a set of simulations with a longer computation domain. However, the required computational demand exceeds our current available computational resource.

4.3. Density Profiles

To provide a more complete statistical description of the stratified wake, this section examines density that varies across the wake in the vertical direction. Figure 7 shows vertical profiles of mean density deviation, $\langle\rho_d\rangle = \langle\rho\rangle - \rho_{bg}$, on the vertical center cut through the wake centerline. It is important to remind ourselves before interpreting the data that the field's density can be measured with respect to $-D^* d\rho^*_{bg}/dz^*$ as we set $d\rho_{bg}/dz = -1$ and $D = 1$ in the simulation, by design. The figure shows that density does deviate from the background state. However, the overall magnitude of the deviation is small and a vertical profile of $\langle\rho\rangle$ itself (not shown) is indistinguishable from that of ρ_{bg}. In the mid-wake ($Nt = 28.3$), density deviation is relatively large in relative to those from $Nt = 54.7$ onward into the far downstream. The vertical extent of nontrivial density disturbances is found to be far beyond the wake boundary ($-2L_V \leq z \leq 2L_V$). Interestingly, in comparison to Fig. 4(a), the influenced area is vertically larger than that of streamwise velocity.

Finally, we provide an evidence in which $\langle\rho_d\rangle$ modifies local stratification, especially in the wake core. Figure 8 shows vertical profiles of vertical gradient of mean density deviation, $\partial_z\langle\rho_d\rangle$, on the vertical center plane.

DOI:10.4186/ej.2021.25.5.1

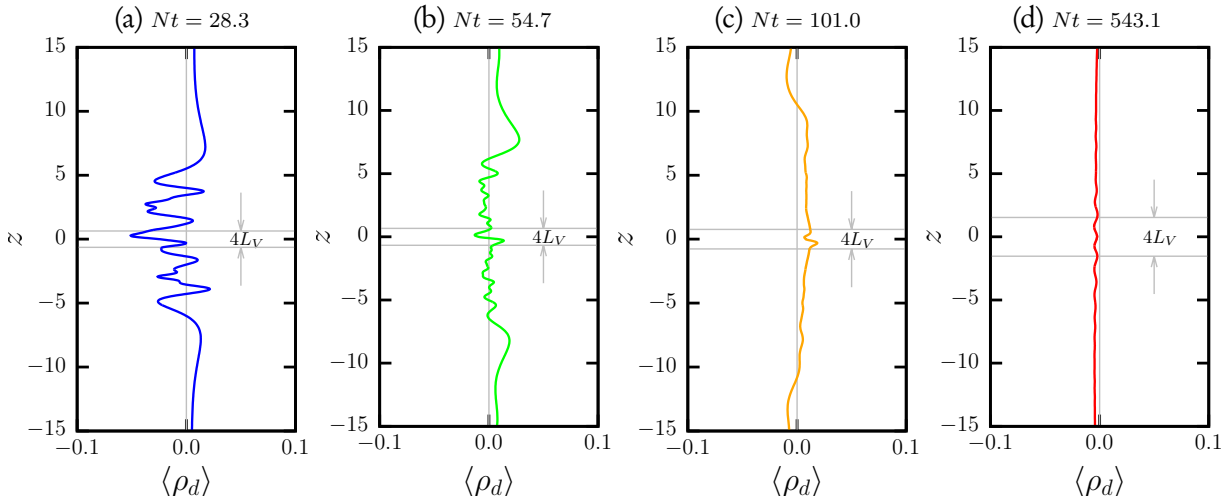

Fig. 7. Vertical profiles of mean density deviation, $\langle \rho_d \rangle = \langle \rho \rangle - \rho_{bg}$, on the vertical center plane at four different downstream locations. The two horizontal gray lines indicate the upper and lower wake boundaries.

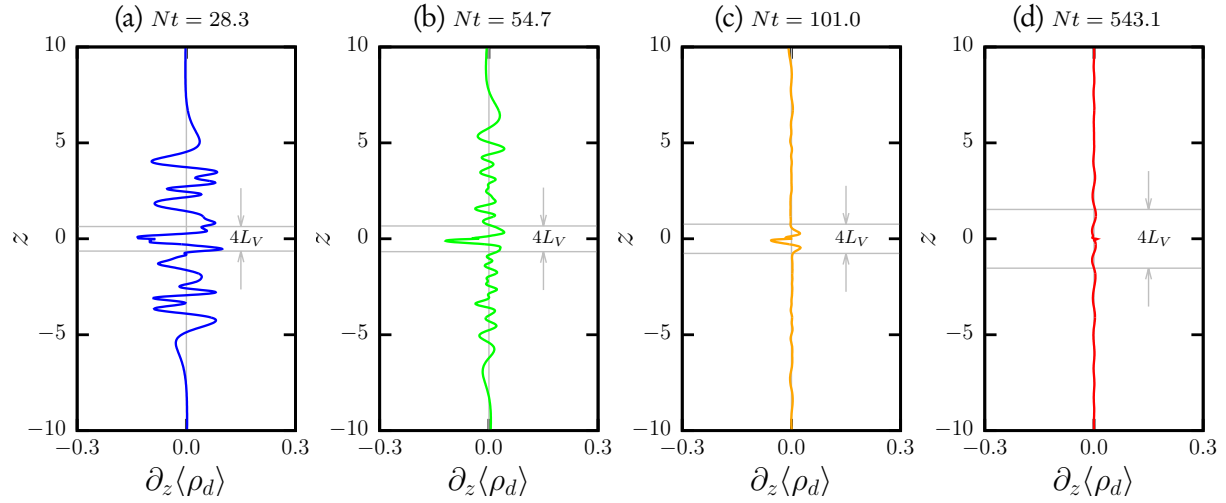

Fig. 8. Vertical profiles of vertical gradient of mean density deviation, $\partial_z \langle \rho_d \rangle$, on the vertical center plane at four different downstream locations. The two horizontal gray lines indicate the upper and lower wake boundaries.

Negative value of $\partial_z \langle \rho_d \rangle$ indicates an increase in density stratification. It is clear that wake core stratification, particularly at the centerline, is enhanced and remains enhanced until about $Nt = 50$ where transitioning into the $Q2D$ regime takes place. Since $d\rho_{bg}/dz = -1$, the enhancement is not small. After the beginning of the transition, viscous diffusion is becoming a dominant mechanism in vertical transport as opposed to the advection by vertical velocity. This allows elements of fluid to return to their density equilibrium and results in the gradual decrease of the centerline enhancement.

5. Summary and Conclusions

Atmospheric pollution, an immediate problem in developing countries, is distributed in density-stratified fluid whose motion is not well understood. The article aims at adding to our comprehension of the evolution of a stratified wake, that is treated as a convenient representation of a decaying patch of turbulence in the density-stratified atmosphere.

Direct numerical simulation (DNS) of stratified wake at relatively low $Re = 10^4$ and moderate $Fr = 3$ has been carried out under the temporal approximation. Initial condition is prescribed based on the data from the body-inclusive simulation of [1] in which the flow ensemble of velocity and density realizations at a single downstream location is stacked the streamwise direction of the present computational volume. The temporal-model simulation then continues to carry the solution onto the far downstream. The ability to carry the wake solution onto the downstream allows a more

confident interpretation of wake statistics as opposed to a simulation whose initial condition is artificially prescribed. Wake statistics is investigated by means of 1) mean streamwise velocity deficit (U_d), 2) vertical half-wake span (L_V), and 3) horizontal half-wake span (L_H).

In the late-NEQ regime (toward the end of the mid wake), centerline mean streamwise velocity deficit continues to evolve with a power-law exponential rate of decay close to $U_0 \propto t^{-0.4}$. Horizontal wake half-width is found to grow with approximately $L_H \propto t^{1/3}$ but vertical wake half-height remains stagnant (i.e., $L_V \propto t^0$).

The NEQ-Q2D transitioning is a gradual process that spans $50 \leq Nt \leq 250$. It is found that the beginning of the transitioning is indicated by the increase in L_V, the decrease in L_H, or can also be indicated by the local minimum of the wake mean geometrical ratio L_V/L_H, which takes place at $Nt = 50$.

In the Q2D regime (the late wake), vertical profile of the mean streamwise defect velocity (U_d) exhibits self-similarity. This self-similar state is not of Gaussian-type but better fitted with individual plane-wake self-similarity solution. The centerline defect velocity rate of decay is promoted to be at $U_0 \propto t^{-3/4}$. The grow rate of wake width is found to be $L_H \propto t^{1/4}$, disagreeing with many previous studies so that its robustness requires further confirmation. However, the required computational demand for further investiation exceeds our current available computational resource. It is found that $L_V \propto t^{1/2}$; the length scale of a pure, viscous diffusion process.

Throughout the wake lifetime, there exists a mean deviation of density from the background state in the vertical center plane. The deviation is small in magnitude but covers larger vertical area than the vertical span of non-trivial velocity deficit. Enchancement in wake-core stratification manifests itself until the NEQ-Q2D transition and gradually decreases afterward.

Acknowledgement

The author would like to thank Professor Sutanu Sarkar for providing the in-house computational resource, located in the Computational Fluid Dynamics Laboratory at University of California San Diego.

References

[1] K. Chongsiripinyo and S. Sarkar, "Effect of stratification on turbulent wake behind a sphere at Re = 10,000," in *Tenth International Symposium on Turbulence and Shear Flow Phenomena (TSFP10), July 6-9, 2017, Swissotel, Chicago-IL, USA*, 2017.

[2] J. T. Lin and Y. H. Pao, "Wakes in stratified fluids," *Ann. Rev. Fluid Mech.*, vol. 11, pp. 317–338, 1979.

[3] G. R. Spedding, "The evolution of initially turbulent bluff-body wakes at high internal Froude number," *J. Fluid Mech.*, vol. 337, pp. 283–301, 1997.

[4] Y. Pao and J. Lin, "Velocity and density measurements in the turbulent wake of a towed slender body in stratified and nonstratified fluids," *Flow Research Inc., Rept*, vol. 12, 1973.

[5] Q. Lin, W. Lindberg, D. Boyer, and H. Fernando, "Stratified flow past a sphere," *Journal of Fluid Mechanics*, vol. 240, pp. 315–354, 1992.

[6] K. Chongsiripinyo and S. Sarkar, "Decay of turbulent wakes behind a disk in homogeneous and stratified fluids," *Journal of Fluid Mechanics*, vol. 885, 2020.

[7] A. M. Abdilghanie and P. J. Diamessis, "The internal gravity wave field emitted by a stably stratified turbulent wake," *J. Fluid Mech.*, vol. 720, pp. 104–139, 2013.

[8] B. R. Sutherland and P. F. Linden, "Internal wave excitation from stratified flow over a thin barrier," *Journal of Fluid Mechanics*, vol. 377, pp. 223–252, 1998.

[9] K. A. Brucker and S. Sarkar, "A comparative study of self-propelled and towed wakes in a stratified fluid," *J. Fluid Mech.*, vol. 652, pp. 373–404, 2010.

[10] K. Chongsiripinyo, A. Pal, and S. Sarkar, "On the vortex dynamics of flow past a sphere at Re= 3700 in a uniformly stratified fluid," *Phys. Fluids*, vol. 29, no. 2, p. 020704, 2017.

[11] S. Nidhan, J. L. Ortiz-Tarin, K. Chongsiripinyo, S. Sarkar, and P. J. Schmid, "Dynamic mode decomposition of stratified wakes," in *AIAA Aviation 2019 Forum*, 2019, p. 3330.

[12] K. Chongsiripinyo and S. Sarkar, "Stratified turbulence in disk wakes," in *Eleventh International Symposium on Turbulence and Shear Flow Phenomena (TSFP11), July 30-August 2, 2019, Southampton, UK*, 2019.

[13] S. Nidhan, K. Chongsiripinyo, S. Sarkar, and O. Schmidt, "Spectral proper orthogonal decomposition of flow around a disk in homogeneous and stratified fluids," *Bulletin of the American Physical Society*, 2019.

[14] D. G. Dommermuth, J. W. Rottman, G. E. Innis, and E. A. Novikov, "Numerical simulation of the wake of a towed sphere in a weakly stratified fluid," *J. Fluid Mech.*, vol. 473, pp. 83–101, 2002.

[15] M. J. Gourlay, S. C. Arendth, D. C. Fritts, and J. Werne, "Numerical modeling of initially turbulent wakes with net momentum," *Phys. Fluids A*, vol. 13, pp. 3783–3802, 2001.

[16] P. J. Diamessis, J. A. Domaradzki, and J. S. Hesthaven, "A spectral multidomain penalty method

model for the simulation of high Reynolds number localized incompressible stratified turbulence," *J. Comput. Phys.*, vol. 202, no. 1, pp. 298–322, 2005.

[17] P. J. Diamessis, G. R. Spedding, and J. A. Domaradzki, "Similarity scaling and vorticity structure in high Reynolds number stably stratified turbulent wakes," *J. Fluid Mech.*, vol. 671, pp. 52–95, 2011.

[18] M. B. de Stadler and S. Sarkar, "Simulation of a propelled wake with moderate excess momentum in a stratified fluid," *J. Fluid Mech.*, vol. 692, pp. 28–52, 2012.

[19] J. A. Redford, T. S. Lund, and G. N. Coleman, "A numerical study of a weakly stratified turbulent wake," *J. Fluid Mech.*, vol. 776, pp. 568–609, 2015.

[20] H. Hanazaki, "A numerical study of three-dimensional stratified flow past a sphere," *J. Fluid Mech.*, vol. 192, pp. 393–419, 1988.

[21] M. B. de Stadler, N. R. Rapaka, and S. Sarkar, "Large eddy simulation of the near to intermediate wake of a heated sphere at Re = 10,000," *Int. J. Heat. Fluid Flow*, vol. 49, pp. 2–10, 2014.

[22] A. Pal, S. Sarkar, A. Posa, and E. Balaras, "Direct numerical simulation of stratified flow past a sphere at a subcritical Reynolds number of 3700 and moderate Froude number," *J. Fluid Mech.*, vol. 826, pp. 5–31, 2017.

[23] J. L. Ortiz-Tarin, K. Chongsiripinyo, and S. Sarkar, "Stratified flow past a prolate spheroid," *Physical Review Fluids*, vol. 4, no. 9, p. 094803, 2019.

[24] R. Pasquetti, "Temporal/spatial simulation of the stratified far wake of a sphere," *Comput. Fluids*, vol. 40, no. 1, pp. 179–187, 2011.

[25] A. VanDine, K. Chongsiripinyo, and S. Sarkar, "Hybrid spatially-evolving DNS model of flow past a sphere," *Comput. Fluids*, vol. 171, pp. 41–52, 2018.

[26] J. Riley, R. Metcalfe, and M. Weismann, "Proc. aip conf. on nonlinear properties of internal waves," 1981.

[27] J. J. Riley and S. M. deBruynKops, "Dynamics of turbulence strongly influenced by buoyancy," *Phys. Fluids*, vol. 15, no. 7, pp. 2047–2059, 2003.

[28] P. Billant and J.-M. Chomaz, "Self-similarity of strongly stratified inviscid flows," *Phys. Fluids*, vol. 13, no. 6, pp. 1645–1651, 2001.

[29] G. Brethouwer, P. Billant, E. Lindborg, and J.-M. Chomaz, "Scaling analysis and simulation of strongly stratified turbulent flows," *J. Fluid Mech.*, vol. 585, pp. 343–368, 2007.

[30] P. Kundu, I. Cohen, and D. Dowling, "Fluid mechanics, 5th version," *Academic, Berlin*, 2012.

[31] S. B. Pope, "Turbulent flows," 2001.

[32] P. Meunier, P. J. Diamessis, and G. R. Spedding, "Self-preservation in stratified momentum wakes," *Physics of Fluids*, vol. 18, no. 10, p. 106601, 2006.

[33] P. Meunier and G. R. Spedding, "Stratified propelled wakes," *Journal of Fluid Mechanics*, vol. 552, pp. 229–256, 2006.

[34] J. Yang and E. Balaras, "An embedded-boundary formulation for large-eddy simulation of turbulent flows interacting with moving boundaries," *J. Comput. Phys.*, vol. 215, pp. 12–40, 2006.

[35] J. Yang, "An embedded-boundary formulation for large-eddy simu- lation of turbulent flows interacting with moving boundaries," Ph.D. dissertation, University of Maryland, College Park, 2005.

[36] G. Spedding, F. Browand, and A. Fincham, "Turbulence, similarity scaling and vortex geometry in the wake of a towed sphere in a stably stratified fluid," *Journal of Fluid Mechanics*, vol. 314, pp. 53–103, 1996.

[37] M. Bonnier and O. Eiff, "Experimental investigation of the collapse of a turbulent wake in a stably stratified fluid," *Phys. Fluids*, vol. 14, no. 2, pp. 791–801, 2002.

[38] D. G. Dommermuth, J. W. Rottman, G. E. Innis, and E. A. Novikov, "Numerical simulation of the wake of a towed sphere in a weakly stratified fluid," *Journal of Fluid Mechanics*, vol. 473, pp. 83–101, 2002.

[39] P. J. Diamessis, G. R. Spedding, and J. A. Domaradzki, "Similarity scaling and vorticity structure in high Reynolds number stably stratified turbulent wakes," *J. Fluid Mech.*, vol. 671, pp. 52–95, 2011.

[40] I. Wygnanski, F. Champagne, and B. Marasli, "On the large-scale structures in two-dimensional, small-deficit, turbulent wakes," *Journal of Fluid Mechanics*, vol. 168, pp. 31–71, 1986.

[41] M. Bonnier and O. Eiff, "Experimental investigation of the collapse of a turbulent wake in a stably stratified fluid," *Phys. Fluids*, vol. 14, no. 2, pp. 791–801, 2002.

[42] M. Bonnier, P. Bonneton, and O. Eiff, "Far-wake of a sphere in a stably stratified fluid: characterization of the vortex structures," *Appl. Sci. Res.*, vol. 59, no. 2-3, pp. 269–281, 1998.

Karu Chongsiripinyo, photograph and biography not available at the time of publication.